Research Paper

Growth rates for freshwater ferromanganese concretions indicate regional climate change in eastern Canada at the Northgrippian-Meghalayan boundary

The Holocene
2021, Vol. 31(8) 1250–1263

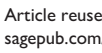

DOI: 10.1177/09596836211011652
journals.sagepub.com/home/hol

Simon Hayles,[1] Tom Al,[1] Jack Cornett,[1] Alex Harrison[1] and Jiujiang Zhao[2]

Abstract

The existence of freshwater ferromanganese concretions has been known for decades, but we are not aware of a generally accepted explanation for their formation, and there has been little research into their potential use as records of Holocene climate and paleohydrology. A conceptual model is presented to describe the environmental and geochemical processes which result in the formation and growth of freshwater ferromanganese concretions. In order to evaluate their potential as historical geochemical records, a concretion from Magaguadavic Lake, New Brunswick, Canada is the focus of a detailed geochronological and geochemical investigation. The radiocarbon data provide a coherent growth curve and a maximum age for the concretion of 8448 ± 43 years, consistent with the establishment of Magaguadavic Lake as a stable post-glacial lacustrine system. The data suggest accretion rates of 1.5 and 3.4 mm per 1000 years during the Northgrippian and Meghalayan stages of the Holocene, respectively. The abrupt change in growth rate observed at the stage boundary may be an indicator of Holocene climate change. These features are consistent with inferences from previous research that warmer climate in the Northgrippian led to eutrophication in some lakes in eastern North America. The results confirm that freshwater Fe–Mn concretions may yield important information about past climatic and environmental conditions.

Keywords

climate, ferromanganese concretions, geochemistry, Holocene, radiocarbon

Introduction

Ferromanganese (Fe–Mn) crusts and concretions (also known as nodules), composed largely of poorly-crystalline and amorphous Fe and Mn oxyhydroxides, have been recovered from the sediment-water interface of the deep oceans, as well as from shallow soils, seas and lakes around the world. Ranging widely in size and shape, deep-marine and soil Fe-Mn concretions tend to be spheroidal with diameters of a few mm to a few 10 s of mm (Crerar and Barnes, 1974; Gasparatos, 2013; Šegvić et al., 2018), whereas concretions from shallow marine and freshwater environments are usually larger (up to hundreds of mm) and tend toward a discoidal shape (Asikainen and Werle, 2007; Sozanski and Cronan, 1976). Post-glacial shallow marine Fe–Mn concretions, such as those found in the Gulf of Bothnia in the Baltic Sea (Glasby et al., 1997; Grigoriev et al., 2004), have morphologies, trace element chemistry and accretion rates that are more similar to lacustrine concretions than to their deep marine counterparts (Trudinger and Swaine, 1979). Growth and preservation of the concretions requires oxidizing conditions and low sedimentation rates (Schoettle and Friedman, 1971).

Freshwater Fe–Mn concretions, hereinafter referred to as concretions, have been reported from Britain (Calvert and Price, 1970; Gorham and Swaine, 1965), North America (Asikainen and Werle, 2007; Beals, 1966; Belzile et al., 2001; Cronan and Thomas, 1970; Dean, 1970; Gillette, 1961; Harriss and Troup, 1970; Kindle, 1935; Medcof, 1979; Rossmann and Callender, 1968; Schoettle and Friedman, 1971; Sommers et al., 2002; Sozanski and Cronan, 1976), Tasmania (Tyler and Buckney, 1980), Japan (Takamatsu et al., 1985), Africa (Williams and Owen, 1992), Russia (Takamatsu et al., 2000), and the Baltic Shield (Dauval'ter and Il'yashuk, 2007). Ranging in size from tens to hundreds of millimeters, concretions commonly form large, irregular, discoidal domed plates around a pebble nucleus (Asikainen and Werle, 2007; Beals, 1966; Harriss and Troup, 1970; Medcof, 1979; Sommers et al., 2002; Sozanski and Cronan, 1976) although a number of different morphologies have been reported including crusts, which Sozanski and Cronan (1976) attribute to the growing together of individual concretions over time. In addition to amorphous oxyhydroxides, X-ray diffraction (XRD) studies reveal that todorokite and birnessite are the most common Mn minerals while Fe is reported to form ferrihydrite, feroxyhyte, and goethite (Callender, 1973; Lee and Xu, 2016; Lee et al., 2016; Schoettle and Friedman, 1971; Sozanski and Cronan, 1979). Freshwater concretions have been shown to have higher Fe/Mn ratios than those from the marine environment as well as

[1]Department of Earth Sciences, Advanced Research Complex, University of Ottawa
[2]Chinese Academy of Geological Sciences, Beijing

Corresponding author:
Simon Hayles, Department of Earth Sciences, Advanced Research Complex, University of Ottawa, Ottawa, ON K1N 6N5, Canada.
Email: shayl019@uottawa.ca

lower concentrations of many minor metals (Price and Calvert, 1970; Schoettle and Friedman, 1971). Previously, in addition to Fe and Mn, geochemical results reported for freshwater concretions have been limited to the major cations and/or metals of potential economic importance (Schoettle and Friedman, 1971; Sozanski and Cronan, 1979), although Edgington and Callender (1970) measured a larger suite of 20 elements, including As, Ba, Ce, Eu, La, Sm, Sr, Th, and U in concretions from Lake Michigan. Barium was also measured in concretions from Oneida Lake, New York, USA (Moore et al., 1980), Pb and Hg are reported for concretions from three lakes in Nova Scotia, Canada (Harriss and Troup, 1970), and partial rare earth element (REE) data are reported for concretions from Lake Shebandowan, Ontario, Canada (Calvert and Price, 1977). All concretions are known to accumulate trace elements and they may represent important sequestration substrates for anthropogenic pollutants (Edgington and Callender, 1970; Suess and Djafari, 1977).

Accurate knowledge of the ages and accretion rates of concretions is vital to developing an understanding of their growth mechanisms and the geochemical conditions of their environment through time. Schoettle and Friedman (1971) collected concretions from Lake George, New York, USA for ^{14}C analysis using bulk samples representative of whole concretions which gave an average age of $3{,}316 \pm 475$ years. Krishnaswami and Moore (1973) analyzed a pair of concretions for Th, Ra and Pb isotopes, one from Lake Alstern in Sweden and the other from Oneida Lake, New York, USA. Both concretions contained relatively high concentrations of ^{226}Ra at the outer rim, decreasing exponentially with distance from the rim to the nucleus, representing a decay curve corresponding to accretion rates of 1 to 3 mm per 1000 years and an age of about 6500 years, assuming a constant source of ^{226}Ra and no ^{226}Ra mobility. A more systematic study of concretions from Oneida Lake was conducted by Moore et al. (1980). In total, one spheroidal and five discoidal concretions were sectioned, sampled along the growth direction and analyzed for ^{226}Ra and ^{210}Pb. Accretion rates were estimated to range from 6 to 11 mm per 1000 years and the maximum ages of the largest concretions (~150 mm diameter) were estimated to be equivalent to the age of the lake (10,000 years). Despite this previous work, few coherent high-resolution geochronological data have been reported.

The source of Fe, Mn and other elements has been discussed in previous literature. Manheim (1965) proposed a link between concretion environment and metal source suggesting that deep-sea concretions formed by oxidation and precipitation of dissolved metals from the water column while shallow-water concretions formed by diagenetic remobilization of metals in sediment porewater. Alternatively, Boudreau (1988) developed a mass-transport model describing the growth processes for discoidal concretions which attributes the source of metals to the water column, and a diagenetic model (Boudreau, 1999) based on the reductive dissolution of metals transported into the sediment column by bioturbation.

Kindle (1935), Gillette (1961), Gorham and Swaine (1965), and Tyler and Buckney (1980) have all suggested the involvement of metal-metabolizing (oxidizing and/or reducing) microbes in the formation of concretions. Recent evidence from the deep oceans strongly suggests a role for metal-metabolizing microbes in the growth and development of Fe–Mn nodules (Lysyuk, 2008; Nayak et al., 2013; Tully and Heidelberg, 2013; Wang et al., 2009). Given the known ubiquity of metal-metabolizing microbes in the lacustrine environment (Fortin et al., 1997; Gregory and Staley, 1982; Nealson and Myers, 1992), as well as evidence for the active involvement of microbes in freshwater Fe and Mn cycling (Chapnick et al., 1982; DiChristina and DeLong, 1993; Ghiorse, 1984; Gounot, 1994), growth models for freshwater Fe-Mn concretions should include biogenetic processes. Recent studies of freshwater concretions indicate that metal-metabolizing microbes are involved in the oxidation of Fe and Mn and subsequent precipitation of the Fe and Mn oxyhydroxide minerals (Sommers et al., 2002; Stein et al., 2001).

Despite the previous work noted above, many questions remain regarding the age and evolution of these concretions, and their potential to provide proxy records of paleo-environmental conditions. Currently available models of concretion formation do not provide a complete explanation for the development of the commonly observed features and morphologies. High-resolution geochronological and geochemical analyses are not yet available, and the potential for the geochemistry of freshwater concretions to provide indications of past environmental and climatic conditions has not yet been explored. The objectives of this study are: (1) to develop a conceptual model that explains the growth and development of freshwater concretions, (2) to collect spatially resolved geochronological data to constrain their age and accretion rates, and (3) to expand existing knowledge of their geochemical characteristics, particularly as records of past environment and climate change.

Sample locations

In the course of this research, ferromanganese concretions have been sampled from six lakes in southern New Brunswick, Canada: Magaguadavic Lake, Harvey Lake, Lake George, Lake Utopia, Oromocto Lake, and Yoho Lake. Based on observations from those lakes, representative concretions from two lakes were selected as the focus for this study. Concretions HL-1 and ML2014 are from Harvey Lake and Magaguadavic Lake (Figure 1) which are at altitudes of approximately 120 and 140 m above mean sea level, 40 and 50 km SW of Fredericton, respectively. Concretion ML2014 (Figure 2) was selected for its relatively large radius and thickness which allow for high-resolution sampling and was the focus of all detailed geochemical investigations. Concretion HL-1 is used to illustrate the structural features that are commonly observed in freshwater concretions. The concretions are found on glacial till at water depths between 3 and 5 m. In the northwest, Magaguadavic Lake is underlain by the Early Devonian Hawkshaw Granite (Figure 1), and in the southeast, it is underlain by low-grade marine metasedimentary rocks, mainly greywacke and slate of the Silurian Kingsclear Group (Balzer and Broster, 1994). Harvey Lake is underlain by the Kingsclear Group to the northwest and by rhyolite of the Late Devonian Harvey Group to the southeast (Dostal et al., 2016). Red-bed sandstones and mudstones of the Carboniferous Mabou and Pictou groups occur in the southeast of the study area (Ryan et al., 1991; St Peter, 1993; Utting et al., 2010). The Mabou Group comprises fine-grained red-beds with thin interbedded sandstone units overlain by thick units of grey sandstone interspersed with red and grey mudstones (Utting et al., 2010), while the Pictou Group comprises grey or red quartz- and feldspar-rich sandstones with a silt or calcite-rich matrix interstratified with red or grey-green mudstones (St Peter, 1993). Exposed bedrock is commonly weathered to depths of more than 1 m (Balzer and Broster, 1994). In most places, the bedrock is overlain by a thin (<0.5 m) sheet of Wisconsinan glacial till that is similar in composition to the underlying bedrock, the matrix varying from dense granitic sand to a compact silty sand with abundant Silurian metasedimentary clasts (Broster and Seaman, 1991).

Methodology

Concretion growth structure

Concretions were collected from the lakebed during scuba dives by one of the authors. The concretions were air-dried and then polished thin-sections were prepared at the University of New Brunswick. The thin-sections were thinly coated with carbon

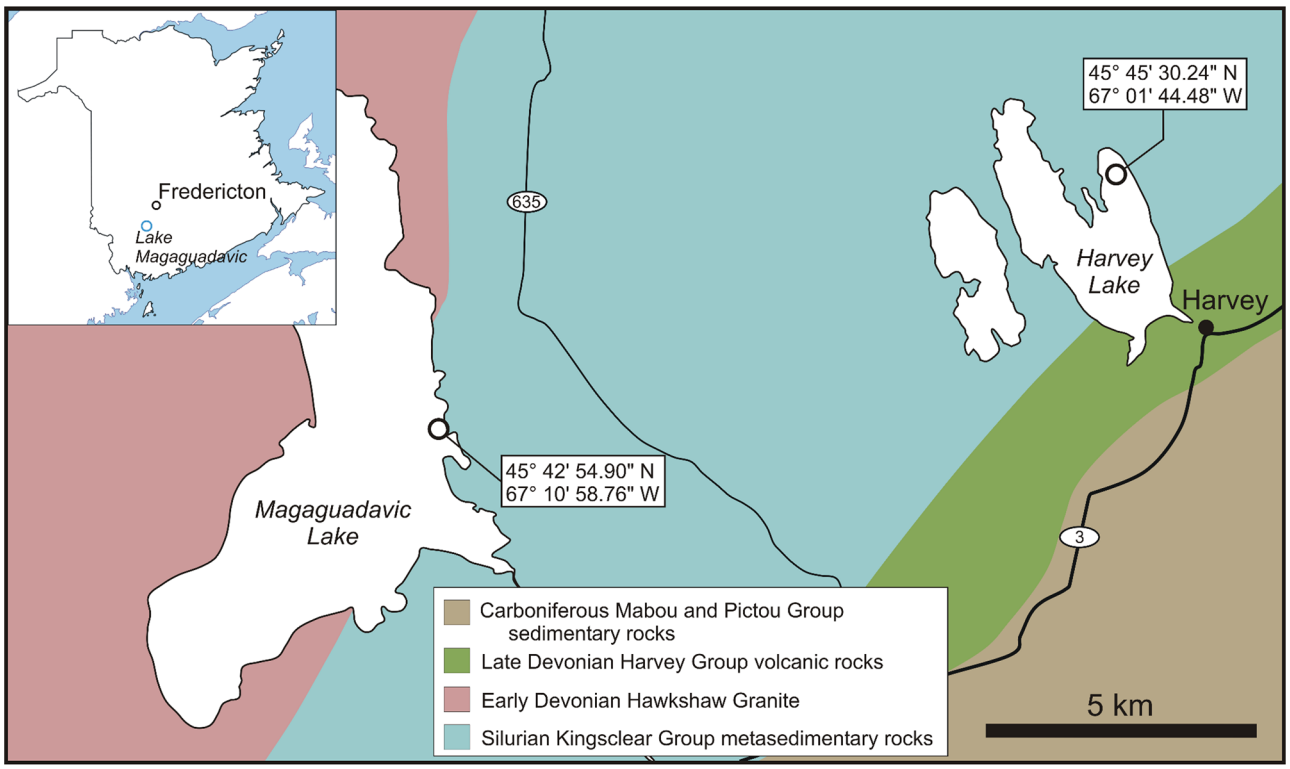

Figure 1. Locations of Magaguadavic Lake and Harvey Lake showing the bedrock geology (Fyffe et al., 2005) and the sampling sites indicated by open circles.

Figure 2. Upper surface (top photo) and lower surface (bottom photo) of Fe–Mn concretion ML2014 from Magaguadavic Lake, New Brunswick, Canada. A lithic fragment forms the central nucleus. The surrounding brown-black material is the concretion, comprised mostly of Fe and Mn oxyhydroxides.

under vacuum to eliminate surface charge accumulation and examined at the University of Ottawa using a JEOL 6610LV scanning electron microscope (SEM) equipped with a large-area silicon drift detector (SDD, Oxford INCA) allowing qualitative energy dispersive X-ray spectrometry (EDS) analysis. EDS spectra were collected under high-vacuum at 15 kV with a beam size of <1 µm.

Concretion subsampling

A water-cooled saw fitted with a diamond blade was used to cut a rectangular segment from concretion ML2014 with dimensions approximately 20 mm thick × 30 mm wide × 50 mm deep extending from the outside edge to the nucleus. The upper and lower surfaces of the concretion segment were removed to a depth of approximately 5 mm using a Dremel rotary tool and diamond bit to eliminate any contamination from recent organic carbon. Twelve sequential samples were then collected from the outer rim of the segment toward the nucleus at 2 mm resolution (~0.5 g) using the rotary tool. The 2 mm sample interval represents a large time interval, so an additional sample (~0.5 g) was subsequently collected from around the extreme outside edge (<1 mm depth) of the concretion in order to establish a radiocarbon age for the most recently accreted material. Each sample was ground to a fine powder using an agate mortar and pestle and divided into subsamples for radiocarbon and geochemical analysis. The additional sample from the rim of ML2014 was only analyzed for radiocarbon.

Radiocarbon analysis

Samples (~0.25 g) were treated to remove inorganic carbonate by adding 5 mL of 1N HCl and heating to 80°C for 30 min, followed by centrifuging at 3000 rpm for 5 min. The supernatant was decanted and three successive washes were conducted with 6 mL of MilliQ water to remove the acid. The samples were freeze dried in a vacuum for 12 h. On weighing the dried samples, it was noted that acidification had resulted in a 2% mass loss (average). Each sample was sealed into a small tin boat, together with a small amount of tungsten-oxide powder used as an ignition agent, and combusted at 1100°C in a Thermo Scientific FlashEA 1112 element analyzer whereupon the CO_2 produced was collected in flame-sealed borosilicate tubes. Carbon from the CO_2 was then graphitized on a custom-built line at the University of Ottawa (St-Jean et al., 2017), compressed along with iron filings into pellet targets, and sent to the A. E. Lalonde AMS laboratory (Kieser

et al., 2015) at the University of Ottawa, Canada for analysis. The radiocarbon was analyzed using a 3.0 MV accelerator mass spectrometer (High Voltage Engineering); ions of ^{12}C, ^{13}C, and ^{14}C were measured using terminal voltages of 2.5 MV and the fraction modern carbon ($F^{14}C$) is defined (Reimer et al., 2004) as the ratio of the sample $^{14}C/^{12}C$ to the standard $^{14}C/^{12}C$ ratio (Ox-II standard). Sample and standard ratios are background corrected and the results are further corrected for spectrometer fractionation using the AMS measured $^{13}C/^{12}C$ ratio. The sample ages are calculated according to Stuiver and Polach (1977) using -8033 ln ($F^{14}C$) and reported as ^{14}C years BP (P = AD 1950) while errors on ^{14}C ages (1σ) are based on counting statistics.

Mineralogy

The mineralogy of the concretions was investigated by X-ray diffraction (XRD), using a Rigaku Ultima IV diffractometer equipped with a Cu source, a diffracted-beam monochromator and a scintillation detector. Two samples of a single concretion from Harvey Lake, NB were analyzed, one from the outer (youngest) region and a second from the inner (oldest) region of the concretion. Measurements were conducted with source voltage and current of 40 kV and 44 mA, a 10 mm divergence slit, a step size of 0.02° 2θ, a scan rate of 0.25°/min and a range from 5 to 60° 2θ. Phase identification was conducted by comparison with the American Mineralogist Crystal Structure Database (Downs and Hall-Wallace, 2003).

Geochemical analysis

Sulphur analyses were conducted with an elemental analyzer (vario Isotope cube, Elementar, Germany). Major, minor and rare earth element analyses were performed by ICP-MS on eleven samples from concretion ML2014 and on two USGS manganese nodule reference material standards (NOD-A-1 and NOD-P-1). The finely-ground samples (~30 mg) were digested overnight in 1.5 mL HNO_3 (SCP PlasmaPure Plus, 60%–73%) and 0.5 mL HCl (Fisher Optima, 32%–35%) at 90°C followed by evaporation to dryness. Next, 0.5 mL HF (SCP PlasmaPure Plus, 47%–51%) were added followed by heating at 90°C for 30 min to ensure complete digestion of all solid material, followed again by evaporation to dryness. Two mL of HNO_3 were added, followed by heating to 90°C and then the solution was again evaporated, this step repeated three times. Finally, 2 mL of HNO_3 were added and the solution heated to 90°C for 30 min at which time the solution was diluted to 10 mL with MilliQ water and again by a factor of 100 with 1% HNO_3. Solutions were prepared from two certified reference solutions (*Enviro*MAT Groundwater, Low [ES-L-3] and High [ES-H-3]) and both instrument and method blanks were also prepared. The solutions were analyzed by ICP-MS at the University of Ottawa (Agilent Technologies 8800 ICP-QQQ). Analytical accuracy calculated from the average differences between measured and certified values from five replicate measurements of 19 elements in the low-concentration groundwater standard (ES-L-3) ranges from 4.3% to 26.3% with a mean of 9.8% and in the high-concentration standard (ES-H-3) the corresponding range is 2.2% to 26.8% with a mean of 8.8%. Analytical precision (relative standard deviation, RSD) for the same measurements ranges from 1.3% to 11.5% with a mean of 8.3% for ES-L-3 and from 2.2% to 7.3% with a mean of 3.9% for ES-H-3. Methodological accuracy calculated as the average differences between measured and certified values from three replicate measurements of 15 elements in each of the USGS reference material standards ranges from 2.1% to 35.5% with a mean of 11.9% for NOD-A-1 and from 4.6% to 30% and a mean of 12.5% for NOD-P-1, while precision for these measurements ranges from 3.3% to 8.0% with a mean of 6.4% for NOD-A-1, and from 12.3% to 34.8% with a mean of 26.4% for NOD-P-1. Method detection limit (MDL) values (3σ) were determined from replicate measurements on the blanks. The REE concentration values were normalized using the Post-Archean Australian Shale (PAAS) data from McLennan (1989).

Results

Observations of concretions from four different lakes in New Brunswick, Canada, indicate that in most cases their morphologies can be described in terms of three main features: a basal Fe-rich zone, a radial growth zone and an upper low-density zone (Figure 3a). The black regions in the back-scattered electron images (BSEI) represent voids in the concretion that have been infilled with epoxy prior to preparing the thin section. It is clear from Figure 3a and b that void space is most abundant in the upper low-density zone. The full extent of the radial growth zone, from the nucleus to the outer rim, is apparent in Figure 3a, and the detailed structure of the growth layers is evident in Figure 3b and in the inset in Figure 3a. The elemental maps in Figure 3c illustrate the Mn-rich composition of the upper low-density zone, the Fe-rich composition of the basal layer and the alternating Fe and Mn layers in the radial growth zone. The Fe-rich layers propagate intermittently upward from the basal Fe-rich zone into the radial growth zone.

Concretion age and accretion rate

The radiocarbon data from ML2014 provide ages that range from younger than AD 1950 at the outer rim of the concretion, to 8,448 ± 43 years BP adjacent to the nucleus (Table 1, Figure 4). The data indicate anomalies at 6 and 16 mm distance from the outer edge of the concretion where the radiocarbon age is younger than the surrounding data points. Although the outer surface of the concretion was cleaned prior to subsampling, these anomalies can best be explained by small amounts of modern carbon contamination. The inverse of the slope represents the accretion rate. It is not uniform over the 8448-year duration; instead, it displays two periods of near uniform accretion rate: 1.5 mm per 1000 years between 8448 and 4683 yr BP and 3.4 mm per 1000 years between 4224 and 826 yr BP.

Mineralogy

The XRD patterns from the concretion samples are presented in Figure 5. The prominent and well-defined peaks represent quartz and albite, both of which are detrital minerals that are also evident in the images presented in Figure 3. They are particularly common in the upper low-density zone. Diffraction peaks related to the Fe and Mn oxyhydroxide minerals are less well defined, the most prominent being a broad peak centered at 37° 2θ, with smaller, poorly defined peaks at 12.3, 21.1, 26.9, 27.6, 33.4, 40.0, 41.3, and 53.5° 2θ. The broad peak centered at 37° 2θ is partly attributable to goethite, FeO(OH), peaks for which also occur at 21.1, 33.4, and 53.4° 2θ. The patterns do not show evidence for the presence of any other Fe oxyhydroxide minerals. There are a number of Mn oxide minerals that could contribute to the broadening of the peak at 37° 2θ, but most have been eliminated because their principal peaks, which should occur at other positions, are absent. However, romanechite, $Ba_{.66}(Mn^{4+}, Mn^{3+})_5O_{10}\cdot 1.34H_2O$, and hausmannite, $Mn^{2+}Mn^{3+}{}_2O_4$, are good fits, and pyrochroite, $Mn(OH)_2$, is also possible, although there is no indication of a pyrochroite peak that is expected at 19.4°2θ. Broad peaks consistent with romanechite are also evident at 26.9, 27.6, 40.0, 41.3, and 53.6° 2θ. The peaks at 26.9 and 27.6° 2θ are best evident in the lower

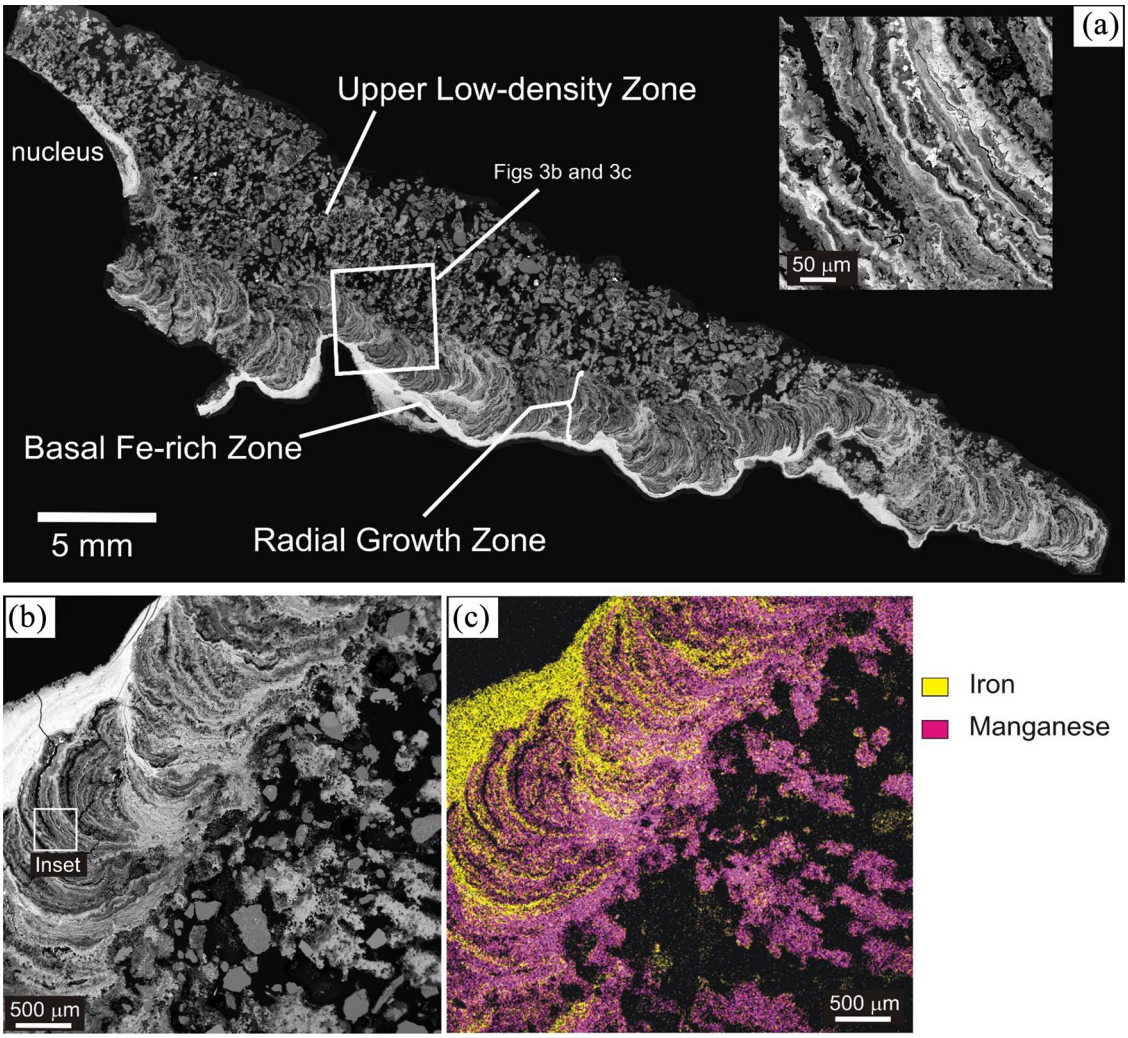

Figure 3. (a) Back-scattered-electron image (BSEI) for a cross-section of a concretion from Harvey Lake, NB, showing the three principle structural features that are common to many concretions. The growth direction is from left to right – the pebble nucleus was located at the arcuate boundary along the left side. The location for the inset image is indicated by the white box in (b). (b) BSEI from the area defined by the white box in (a). From top left to bottom right, the basal Fe-rich zone is evident at the top left, the radial growth zone is in the middle and the upper low-density zone occurs at the right side. (c) Composite element map for Fe (yellow) and Mn (magenta) acquired with SEM-EDS.

Table 1. Results of radiocarbon analysis.

Sample ID	Depth (mm)	±	$F^{14}C$	±	^{14}C (yr BP)	±
ML2014-1-00	0.5	0.5	1.0204	0.0029	>Modern	23
ML2014-3-01	2	1.5	0.9023	0.0032	826	29
ML2014-3-02	4	1	0.7400	0.0023	2418	25
ML2014-3-03	6	1	0.7564	0.0027	2243	29
ML2014-3-04	8	1	0.6595	0.0024	3344	29
ML2014-3-05	10	1	0.6362	0.0029	3633	36
ML2014-3-06	12	1	0.6029	0.0023	4065	31
ML2014-3-07	14	1	0.5911	0.0034	4224	46
ML2014-3-08	16	1	0.6404	0.0022	3580	35
ML2014-3-09	18	1	0.5583	0.0039	4683	56
ML2014-3-10	20	1	0.5068	0.0022	5460	35
ML2014-3-11	22	1	0.4070	0.0034	7220	68
ML2014-3-12	24	1	0.3494	0.0019	8448	43

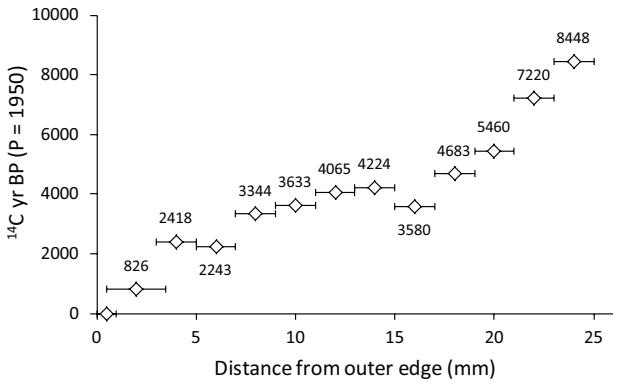

Figure 4. Plot of radiocarbon dates against distance from the outer edge of the concretion toward the nucleus. The error bars represent the thickness of individual samples. Error bars for the Y-axis are smaller than the symbols.

pattern where the adjacent albite peak is relatively small. Hausmannite is evident only by its principal peak at 36.13° 2θ, and it appears to be present only in the lower pattern where it contributes to a greater amount of broadening for the 37-degree peak compared to the upper pattern. The presence of birnessite, $(Na,K,Ca)Mn_7O_{14}{\cdot}2.8H_2O$, is evident in both samples, but most clearly in the upper pattern. It is manifest by a broad peak centered at 12.3° 2θ.

Major and trace element geochemistry

Attempts to measure the concentration of S in the concretions with elemental analysis obtained values below the method

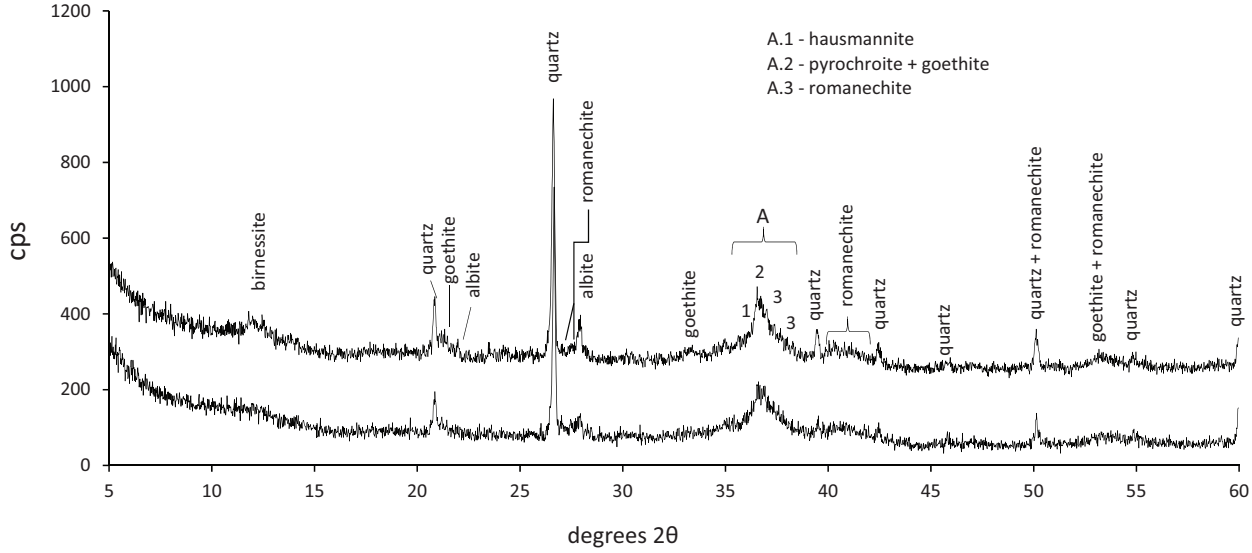

Figure 5. X-ray diffraction patterns from a concretion collected from Harvey Lake, New Brunswick. The upper pattern represents material from the inner, or oldest, segment of the concretion, and the lower pattern represents the outer segment.

Table 2. Major and selected trace element composition (ppm).

Sample ID	^{14}C Age	Al	As	Ba	Ca	Fe	K	Mg	Mn	Na	Sr	Zn	Fe/Mn
ML2014-3-01	826	16,671	367	9,811	11,863	172,714	113,97	1,783	290,570	13,002	249	863	0.59
ML2014-3-02	2,418	9,966	428	7,829	7,567	370,466	2,114	821	228,050	2,245	332	273	1.62
ML2014-3-03	2,243	11,637	243	8,431	11,831	197,907	11,496	1,049	287,696	14,666	361	406	0.69
ML2014-3-04	3,344	11,417	516	8,012	8,335	421,938	11,181	860	268,445	3,704	733	303	1.57
ML2014-3-05	3,633	12,289	319	7,840	10,296	230,185	25,399	1,453	270,293	23,491	632	336	0.85
ML2014-3-06	4,065	8,901	341	6,590	9,201	264717	6,517	880	249,893	4,296	475	273	1.06
ML2014-3-07	4,224	12,037	360	11,196	10,522	251,345	17,856	1,248	321,273	18,968	700	377	0.78
ML2014-3-08	3,580	9,564	349	10,846	7,961	224,773	15,557	1,038	264,641	9,675	772	391	0.85
ML2014-3-09	4,683	10,571	665	12,510	8,896	435,130	34,341	1,486	365,027	16,385	1,946	295	1.19
ML2014-3-11	7,220	8,062	386	14,894	8,033	178,281	44,319	1,522	327,970	15,998	1,689	184	0.54
ML2014-3-12	8,448	5,044	361	9,784	8,925	164,161	40,323	2,064	336,659	10,330	1,979	108	0.49
Mean	–	10,560	394	9,795	9,403	264,692	20,046	1,291	291,865	12,069	897	346	0.93
Std dev	–	2,918	112	2,438	1,516	99,207	14,104	407	41,395	6,748	652	193	0.39
MDL	–	0.054	0.0011	0.0026	0.0762	0.10	2.35	0.0533	0.157	0.594	0.002	0.007	–

detection limit (100 ppm). The mean Fe and Mn concentrations are 26.5 wt% and 29.2 wt% respectively (Table 2); as oxides (Fe_2O_3 and MnO_2), Fe and Mn represent 84.2% of the total sample mass. Iron concentrations range more widely (16.4 wt% to 43.5 wt%) than those of Mn (22.8 wt% to 36.5 wt%) and there are no apparent trends with respect to radiocarbon age. The Fe/Mn ratio ranges from 0.49 to 1.62, reflecting mm-scale heterogeneity in the acquired chemical and mineralogical composition of the concretions versus time. There is variability in the concentrations of all the major and trace elements, but in most cases there are no clear trends with radiocarbon age (Table 2). Strontium is the one exception, with concentrations ranging from 1979 ppm in the sample with the oldest radiocarbon age, to 249 ppm in the youngest sample. Notably, Ba concentrations are high, ranging from 6590 to 14,894 ppm with a mean of 9800 ppm.

While all the REE can exist in a trivalent state, the valence of Ce and Eu changes according to the redox environment; Ce varying between Ce(III) and Ce(IV) and Eu varying between Eu(II) and Eu(III), resulting in fractionation of these elements from the series. The magnitude of the Ce and Eu fractionation, commonly referred to as Ce or Eu anomalies, is evaluated by comparing the measured Ce and Eu concentrations to their respective interpolated (unfractionated) concentrations. Values for the Ce anomalies (Ce_{an}) are calculated according to:

$$Ce_{an} = Ce_{norm} / \left(La_{norm} \times Pr_{norm} \right)^{0.5} \quad (1)$$

and values for the Eu anomalies (Eu_{an}) are calculated according to:

$$Eu_{an} = Eu_{norm} / \left(Sm_{norm} \times Gd_{norm} \right)^{0.5} \quad (2)$$

where Ce_{norm}, La_{norm}, Pr_{norm}, Eu_{norm}, Sm_{norm}, and Gd_{norm} are the respective normalized measured concentrations.

Measured concentrations of Ce range from 34 to 259 ppm with a mean of 135 ppm, while for Eu the range is 2.8 to 4.8 ppm with a mean of 3.6 ppm. When the Ce and Eu anomalies are plotted against radiocarbon age (Figure 6), trends are apparent. The Ce_{an} is lowest (0.61) in the sample with the oldest radiocarbon age and increases gradually through the Northgrippian, while through most of the Meghalayan Ce_{an} is near unity, but there is a steep increase toward the highest value (2.15) in the single sample with the youngest radiocarbon age. The Eu_{an} values (Figure 6) are all positive, with the highest values (3.21) recorded in the sample with the oldest radiocarbon age. Values for Eu_{an} decrease with

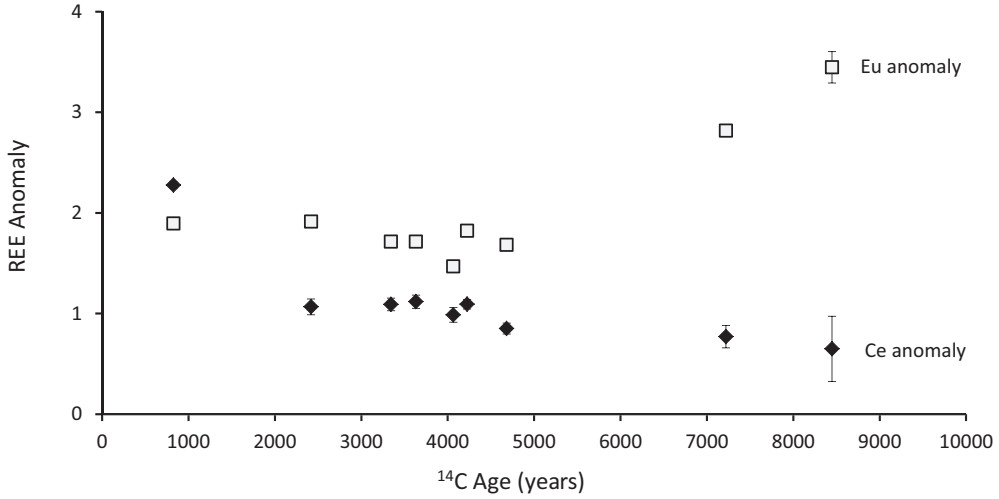

Figure 6. Plot of Ce and Eu anomalies for concretion ML2014 against ^{14}C age. Error bars represent analytical error but the error bars for the horizontal axis are smaller than the symbols.

time, reaching a minimum value of 1.37 at the end of the Northgrippian, after which they are relatively constant, ranging between 1.6 and 1.8.

Discussion

Concretion age and accretion rate

The radiocarbon data (Table 1, Figure 4) provide a maximum age of 8448 ± 43 years. The growth period of several thousand years demonstrates that the locations on the lake bottom where the concretions occur are areas where there is no net sedimentation. Patterson et al. (2020) conducted investigations of the maximum depth at which sediments in Harvey Lake will be disturbed by wave action driven by storms and high-winds. They determined that the maximum wave base depth is around 6 m in Harvey Lake and, given that this depth is largely controlled by local weather, it is likely that the storm wave base for Lake Magaguadavic is similar. From our observations, most concretions are found at depths less than the maximum wave base where sediment is subject to resuspension and transport to deeper regions in the lake.

Wisconsinan glaciers had begun their retreat from the southern coast of New Brunswick by 15,000 years BP and glacial ice had largely disappeared from New Brunswick by the beginning of the Holocene (Broster and Dickinson, 2015; Honig and Scott, 1987; Shaw et al., 2002). Glacial retreat was followed by isostatic rebound on land and falling relative sea level (RSL) along the southern coast during the early- to mid-Holocene (Honig and Scott, 1987; Quinlan and Beaumont, 1981). Radiocarbon-dated pollen profiles from lakes in SW New Brunswick show that the tundra vegetation which initially followed the ice retreat was replaced by pioneer birch, aspen and spruce forest by 12,000 years BP and, by 9500 years BP, mature forests of pine and oak were dominant (Mott, 1975). The maximum age of ML2014 is therefore consistent with accretion following the establishment of a stable freshwater lacustrine system.

The C measured in geochronological investigation of the concretion is likely the fossil remains of metal-metabolizing microbes, possibly retained in the concretion via self-mediated entombment as described by Tebo et al. (2004). The radiocarbon data define a coherent timeline for growth of the concretion. The slope of the linear best-fit line through all of the radiocarbon ages and the origin gives an average accretion rate of 3.2 mm per 1000 years (Figure 4). This rate compares favorably with accretion rate calculations for lacustrine concretions by other researchers (Krishnaswami and Moore, 1973; Moore et al., 1980). However, the overall best-fit line is not representative of the entire period of concretion growth (Figure 4). Linear regressions using the radiocarbon data from an early growth period (8448 to 4683 years BP) versus a later period (4224 to 826 years BP) yield average accretion rates of 1.5 and 3.4 mm per 1000 years respectively. There are a number of inter-related factors that can influence the accretion rate; the number of ice-free days in the year, availability of dissolved O_2 at the sediment-water interface, temperature, and the flux of Fe and Mn from the sediment porewater – all of these are influenced by climate.

The warm dry conditions which prevailed during the Northgrippian stage (8.2–4.2 kyr BP; Walker et al., 2019) of the Holocene in contrast with the cooler Meghalayan stage (4.2–0 kyr BP; Walker et al., 2019) have been well documented both globally (Jansen et al., 2007; Marcott et al., 2013) and regionally in North America (Dean et al., 1996; Jansen et al., 2008). A study of lake levels over time in Lake Winnipeg, Manitoba, Canada demonstrated an extended period of aridity during the Northgrippian (Lewis et al., 2001), and lakes in Northern Ontario, Canada were affected by water level declines of more than 8 m during the same period (Laird and Cumming, 2008). Odegaard et al. (2003) identified black sulphide-rich bands in Northgrippian sediments for lakes Michigan and Huron indicating extended periods of basin-wide anoxia and low lake levels attributed to the warm dry climate. Reductions in lake levels attributed to the warm dry conditions in the Northgrippian have also been reported from lakes in Ontario, Canada (Yu and McAndrews, 1994; Yu et al., 1997) and Québec, Canada (Lavoie and Richard, 2000), while sea level changes around Nova Scotia, Canada (Scott et al., 1995) are likewise attributed to a warm dry climate during the mid-Northgrippian. By contrast, the Meghalayan was cooler in the Northern Hemisphere (Jansen et al., 2008; Marcott et al., 2013) with advancing glaciers in the mountains (Solomina et al., 2015). It was also increasingly humid in North America (Davis et al., 2000; Jackson and Booth, 2002) during the Meghalayan with higher lake water levels compared with the earlier period (Brugam et al., 1998; Kaufman et al., 2016; Laird and Cumming, 2008; Lavoie and Richard, 2000; Lewis et al., 2001; Yu and McAndrews, 1994).

Contrasting environmental conditions between the Northgrippian and the Meghalayan stages likely account for the observed differences in accretion rates. During the Northgrippian, increased lake productivity in a warmer drier climate, with a longer aquatic growing season, for example, may have contributed to eutrophication (Moss et al., 2011), as has been reported for the mid-Holocene for lakes in New York State, USA (Mullins, 1998) and

Table 3. Geochemical comparison with previously published data.

Ref.	*n*	Fe (%)	Mn (%)	Fe/Mn	As (ppm)	Ba (ppm)	Co (ppm)	Cu (ppm)	Ni (ppm)	Pb (ppm)	Zn (ppm)
1	11	26.5	29.2	0.9	394.1	9794.9	88.0	6.2	25.0	18.0	346.4
2	44	9.0	38.8	0.2	–	23197.4	84.5	108.0	69.6	–	246.6
3	72	42.5	6.3	6.7	–	–	109.0	33.0	105.0	–	261.0
4	7	33.5	3.6	9.4	–	–	220.0	1310.0	700.0	–	1180.0
5	9	15.3	6.5	2.4	121.6	5407.9	51.1	8.3	–	–	144.3
6	33	20.6	17.0	1.2	–	–	643.0	363.0	2385.0	–	1996.0
7	41	16.6	33.0	0.5	–	–	196.0	14.0	296.0	26.0	1665.0
8	19	16.7	26.6	0.6	–	–	221.0	7.0	112.0	27.0	475.0
9	17	40.2	15.7	2.6	–	–	135.0	10.0	95.0	24.0	250.0

[1]This article (Lake Magaguadavic, NB).
[2]Moore et al. (1980) (Lake Oneida, NY).
[3]Sozanski and Cronan (1979) (Lake Shebandowan, ON).
[4]Schoettle and Friedman (1971) (Lake George, NY).
[5]Edgington and Callender (1970) (Lake Michigan, WI).
[6]Cronan and Thomas (1970) (Lake Ontario, ON).
[7]Harriss and Troup (1970) (Grand Lake, NS).
[8]Harriss and Troup (1970) (Ship Harbour Lake, NS).
[9]Harriss and Troup (1970) (Mosque Lake, NS).

Northern Ontario, Canada (Karmakar et al., 2015; Moos et al., 2009), and suboxic conditions which would in turn slow the rate of oxidative Fe and Mn precipitation and concretion growth. In addition, lower water levels would have diminished the hydraulic gradients that drive Fe(II)- and Mn(II)-rich groundwater fluxes into the lake. Conversely, a cooler more humid climate during the Meghalayan could have resulted in increased Fe(II) and Mn(II) fluxes to the lake with groundwater, and greater O_2 availability, creating conditions suited to the faster accretion rates indicated by the radiocarbon data.

Concretion geochemistry

The geochemical analyses for ML2014 compare well with concretions from North American lakes (Table 3), although other researchers have measured higher Fe/Mn ratios and trace metal concentrations. The average Fe/Mn ratio for ML2014 is closest to the values reported for concretions from Lake Ontario, Grand Lake, and Ship Harbour Lake. Average trace metal concentrations, Cu and Ni in particular, are low in ML2014 compared with other concretions. The compositional variations for concretions from different lakes are likely related to variations in the chemical and mineralogical compositions of local bedrock, glacial drift, and/or lakebed sediments.

Statistical analysis has been conducted with R (R Core Team, 2015) to explore inter-element correlations in the geochemical results (Figure 7). There are positive correlations for As (0.81), Cr (0.88), Pb (0.76), and V (0.81) with Fe. Arsenic is strongly adsorbed to Fe oxyhydroxide surfaces (Pierce and Moore, 1982; Raven et al., 1998; Vitre et al., 1991) and can be extensively recycled with Fe along redox gradients in aquatic systems (Belzile and Tessier, 1990; Couture et al., 2010; Root et al., 2007; Tufano et al., 2008). Similarly, surface sorption and/or co-precipitation processes are likely responsible for the association of the other trace metals with Fe oxyhydroxides (Rai et al., 1987; Sass and Rai, 1987; Tessier et al., 1985, 1996; Trivedi et al., 2003; Wehrli et al., 1989).

There is positive correlation of Ba (0.84), Cu (0.74), K (0.86), Mg (0.84), Ni (0.79), Rb (0.89), Sr (0.86), and U (0.8) with Mn (Figure 7). These geochemical associations may arise due to adsorption mechanisms such as cation exchange or surface complexation, particularly for trace metals such as Cu, Ni, and U (Tessier et al., 1996; Young and Harvey, 1992), but the cations Ba, K, Rb, Sr, and Mg substitute in the crystal structure of Mn-oxyhydroxide minerals that were detected in these concretions (birnessite and romanechite). Cations and water molecules are sequestered within the layer and tunnel structures created by the edge and corner sharing of the MnO_6 octahedra in these minerals. They also contain a mix of Mn(III) and Mn(IV) in order to maintain charge balance with the cations (Post, 1999). The low S content of the concretions demonstrates that Ba and Sr are not present in the form of low-solubility sulphate minerals barite and celestine.

The potential use of fractionations in the REE series as proxies for paleo-redox conditions has long been recognized (e.g. Glasby, 1973; Liu et al., 1988; Piper, 1974). Previous research has demonstrated that in aquatic systems and near-surface sediments, the REE partition preferentially to Fe and Mn oxyhydroxides (German and Elderfield, 1989; Leybourne and Johannesson, 2008; MacRae et al., 1992). Enrichment of REE in Fe-Mn oxyhydroxides, combined with the variable oxidation states of Ce and Eu, suggests that REE concentrations in concretions could be sensitive indicators for the evolution of paleo-redox conditions. The Ce and Eu concentrations in ML2014 compare well with concretions from other North American lakes. In concretions from Lake Michigan, Edgington and Callender (1970) measured Ce concentrations ranging from 55 to 211 ppm with a mean of 144 ppm, and Eu concentrations ranging from 0.3 to 2.6 ppm with a mean of 1.4 ppm. Average Ce and Eu concentrations in concretions from Lake Shebandowan (Calvert and Price, 1977) are 38 ppm and 0.7 ppm respectively.

The Eu_{an} values (Figure 6) are all positive, with the highest values (3.21) recorded in the sample with the oldest radiocarbon age. Values for Eu_{an} decrease with time, reaching a minimum value of 1.37 at the end of the Northgrippian, after which they are relatively constant, ranging between 1.6 and 1.8. It is not possible to completely eliminate detrital feldspar grains from the sample material, so the question arises whether Eu_{an} is reflecting characteristics inherited from the Hawkshaw granite. Geochemical analyses of the parent body for the Hawkshaw granite, the Pokiok Batholith, include only partial REE data (Leonard et al., 2006; Lutes, 1987) precluding the calculation of anomalies. However, other igneous intrusions of Silurian-Devonian age in the region predominantly display negative Eu anomalies (Whalen et al., 1994, 1996; Yang et al., 2008). Furthermore, the pronounced variation in Eu_{an} versus time in ML2014 is not consistent with an inherited signal from detrital minerals derived from the underlying lake sediment.

During the Northgrippian, the observed Ce_{an} and Eu_{an} values suggest the prevalence of relatively reducing redox conditions at the sediment-water interface. This evidence is consistent with the inference made above that lower concretion accretion rates during the Northgrippian may be related to suboxic conditions caused by

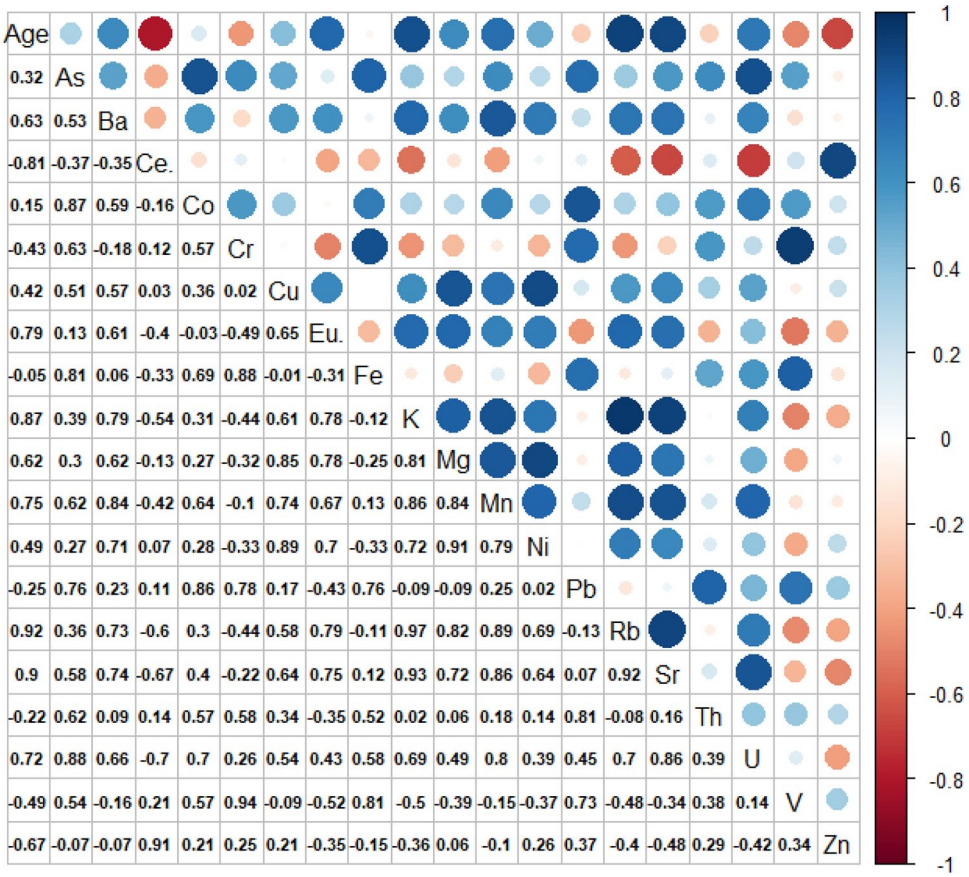

Figure 7. Correlation matrix for ML2014 samples showing 17 measured elements together with ^{14}C age and calculated REE anomalies (using "corrplot" from Wei et al., 2017).

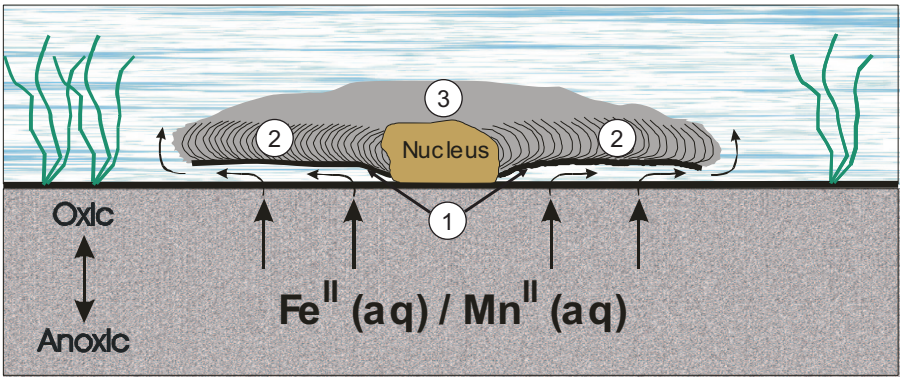

Figure 8. Conceptual model for the formation of freshwater Fe-Mn concretions illustrating: (1) basal Fe-rich zone, (2) radial growth zone, (3) upper low-density zone.

eutrophication. Similarly, values of Ce_{an} near unity, lower Eu_{an} values, and the measured increase in concretion accretion rates during the Meghalayan are consistent with a transition to mesotrophic conditions and greater O_2 availability at the sediment-water interface. The elevated single value for Ce_{an} (2.15) at a radiocarbon age of 826 years BP (Figure 6) suggests that the evolution toward more oxidizing redox conditions may have accelerated in the later Meghalayan.

Concretion growth structure and conceptual model

Growth of the concretions requires a sustained source of Fe and Mn, which might come from the overlying water column and/or the underlying sediment porewater. However, Fe(II) and Mn(II) are not easily transported in O_2-rich, near-neutral pH surface waters (streams and lakes) because they are readily oxidized, and the solubilities of their oxidized species (Fe(III) and Mn(III/IV)) are extremely low (Martin, 2005). Consequently, the oxygenated lake water is an unlikely source for the metals, suggesting that the sediment porewater is the dominant source. Ultimately, the Fe, Mn and trace elements would be derived from the sediments or from groundwater fluxes to the lake. Metals derived from the sediments are released to the sediment porewater by reductive dissolution of their respective oxides and hydroxides – a common diagenetic process in lake sediments (Davison, 1993; Froelich et al., 1979). Once in the porewater, the dissolved metals can migrate by advection and/or diffusion upward to the sediment-water interface (Figure 8). As aqueous Fe(II) and Mn(II) are transported to the sediment-water interface, Fe(II) is expected to oxidize rapidly by chemical or biologically-mediated mechanisms. The biological mechanism is active when the temperature is above 10 to 15°C (Davison and Seed, 1983; Martin, 2005; Millero et al., 1987; St Clair et al., 2019)

and chemical Fe oxidation will dominate at lower temperatures. In contrast, chemical oxidation of Mn(II) is kinetically inhibited at pH below 8 (Martin, 2005) and present-day pH values for these New Brunswick lakes are <7.5 (Government of New Brunswick, 2020). It is not possible to be certain that pH was always lower than eight during the long growth period for the concretions, but Canadian lakes with similar underlying geology generally have near-neutral pH (Dranga et al., 2018), so biologically-mediated oxidation is the only viable mechanism for Mn. However, biological Mn oxidation rates are negligible at temperatures below 8°C to 9°C (Dangeti et al., 2017) so, in temperate climates, Mn(II) oxidation is restricted to the non-winter period.

In most cases, concretions nucleate around pebbles or cobbles of variable lithology. It is likely that growth of concretions is unrelated to the lithology of the nucleus, but the rock provides a solid substrate for growth of a biofilm, which in turn mediates oxidation of Mn(II) and Fe(II). The development of surficial biofilms is described in detail by Little et al. (1997) while Fortin et al. (1997) discuss the processes of metal complexation in biofilms. Oxidation of Fe(II) and Mn(II) at the interface with the nucleus forms low-solubility Fe and Mn oxyhydroxide minerals, and as the concretion continues to grow, some or all of the previously mentioned features appear: the basal Fe-rich zone, the radial growth zone and the upper low-density zone.

Basal Fe-rich zone

Accepting that the sediments, and possibly groundwater, are the dominant sources of Fe(II), Mn(II) and trace elements, and that these solutes are transported upward to the sediment-water interface by diffusion and/or advection, the underside of a pebble (early stage) or concretion (later stage) represents a barrier to the vertical transport of solutes, causing the solute flux to diverge radially (Figure 8). The interface between the base of the concretion and the top of the sediment is not in direct contact with the oxygenated water column so conditions are expected to be suboxic and not ideal for supporting biologically mediated oxidation of Fe(II) and Mn(II). The Fe-rich composition of this basal zone suggests that Fe(II) is oxidized primarily by a chemical mechanism and that virtually all of the Mn(II) flux from the underlying sediment porewater is diverted toward the perimeter of the concretion (Figure 8).

Radial growth zone

As reduced species migrate radially beneath the concretion (Figure 8), oxic lake water is encountered at the perimeter of the pebble or concretion. This perimeter region, effectively a ring-like interface between suboxic conditions below and oxic conditions above, is a region well suited to support a biofilm containing Fe(II)- and Mn(II)-oxidizing chemoautotrophic microorganisms (Erbs and Spain, 2002; Ghiorse, 1984; Little et al., 1997; Tebo et al., 2005). This is the locus for chemically- and/or biologically-mediated precipitation of Fe(III) and Mn(III,IV) oxyhydroxides, and it represents the leading edge of the radial growth zone (Figure 8).

The observed alternating Fe-rich and Mn-rich layers might be expected to form in part due to seasonal, temperature-controlled variations in the metabolic activity of Mn-oxidizing microorganisms (Dangeti et al., 2017). This could result in alternation between Fe- and Mn-rich layers on an annual basis, as has been suggested (Harriss and Troup, 1970; Sozanski and Cronan, 1979). However, the Fe-Mn layering could also result from vertical oscillations in the position of the redox gradient that exists downward through the water column and into the sediment (Davison, 1993; Figure 9). Thermodynamically, the Fe redoxcline [transition from Fe(III) to Fe(II)] will occur deeper in the water or sediment column compared with the Mn redoxcline [transition from Mn(IV) to Mn(II)] and their respective depths will co-vary with dissolved O_2 (DO) near the sediment-water interface (Davison, 1993). A well-mixed water column with high lakebed DO would result in depressed redoxclines such that only Mn(II) reaches the sediment-water interface where it can be oxidized and precipitated at the leading edge of the concretions, while Fe(II) oxidation and precipitation takes place in the upper sediments (Figure 9a). A DO-limited water column, due to prolonged ice cover or high biological productivity, would result in raised redoxclines such that Mn(II) is transported upward into the water column and Fe(II) could be oxidized and precipitated at the leading edge of concretions (Figure 9b). Thus, seasonal temperature variations or vertical oscillations in the redoxcline could explain the alternating Fe and Mn layers.

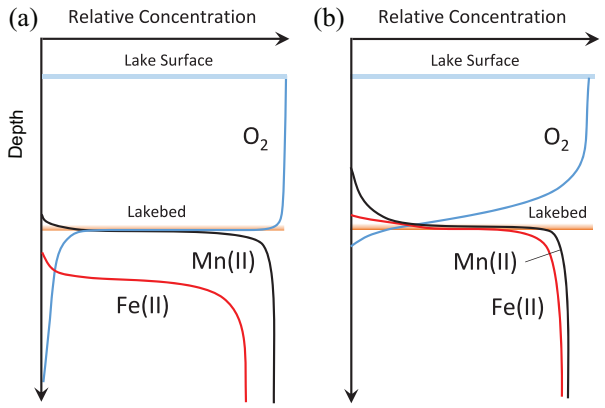

Figure 9. Conceptual diagram representing conditions that would be conducive to (a) Mn accretion, or (b) Fe accretion, at the leading edges of lakebed concretions. The profiles of relative concentration versus depth for O_2, Fe(II) and Mn(II) are not to scale. The concentration profiles for Mn(II) and Fe(II) in the water column above the sediment-water interface are assumed to result from diffusive transport upward from the sediment porewater. Dispersive effects of currents in the water column are not considered.

Upper low-density zone

During the ice-free period when precipitation of Fe and Mn oxyhydroxides is rapid at the sediment-water interface or the leading edge of the radial growth zone (Figure 9a), the concentrations of Fe(II) and Mn(II) in the water column in contact with the upper surface of the concretion should be at a minimum and mineral accretion rates on the upper surface should be negligible. However, during the ice-covered period, the rates of biologically-mediated Mn(II) oxidation and precipitation of Mn oxyhydroxides are expected to decrease significantly, or cease altogether, allowing aqueous Mn(II) to accumulate in the water column (Figure 9b) as observed by Chapnick et al. (1982) in Oneida Lake. In contrast, the chemical oxidation mechanism for Fe(II) is viable at low temperature so corresponding accumulation of aqueous Fe(II) is not expected. After the ice cover disappears and the lake begins to warm, biological Mn(II) oxidation will resume and Mn-oxidizing bacteria on the upper surface of the concretion would be expected to oxidize any aqueous Mn(II) that accumulated over the winter, thereby preferentially accreting Mn-oxyhydroxides and contributing to growth of the upper low-density zone. In addition to the accumulation of Mn oxyhydroxide minerals, the upper low-density zone also contains a relatively large amount of detrital minerals that presumably are deposited due to resuspension of the surrounding sediment by storms or turbulence created by fish.

Conclusions

1. The age and accretion rate of a concretion from Magaguadavic Lake has been determined by radiocarbon measurements at approximately 2 mm spatial resolution; the first time this has been achieved to the best of our knowledge. The radiocarbon data indicates a maximum age of 8448 years BP indicating that its growth extends across the Meghalayan and Northgrippian stages of the Holocene Epoch.
2. Calculated accretion rates are approximately 1.5 mm per 1000 years during the Northgrippian stage of the Holocene (8200 to 4200 years BP), and a faster rate of approximately 3.4 mm per 1000 years during the Meghalayan stage (4200 years BP until the present).
3. It is proposed that the slower accretion rate during the Northgrippian may be due to the prevalence of eutrophic conditions induced by the relatively warm climate compared to the Meghalayan stage. This inference is supported by Ce and Eu anomalies that suggest paleo-redox conditions were relatively reducing during the Northgrippian.
4. A conceptual model is proposed to explain the formation of freshwater ferromanganese concretions. It is based on observations of many concretions from lakes in southwest New Brunswick, Canada, combined with electron microscopy investigations of their internal structural and chemical properties.

Acknowledgements

Our grateful thanks to the highly professional team of technicians and laboratory scientists at the Advanced Research Complex at the University of Ottawa for their willingly given time, energy and expertise. This work was funded through an NSERC Discovery Grant to TA (Grant #147654). A special thank you goes to Dr. D. Fox at the New Brunswick Department of Environment and Local Government who first introduced TA to the occurrence of freshwater ferromanganese concretions. We thank the anonymous reviewers and the editor, Dr. Sandra Passchier, for their helpful comments.

Dedication

We dedicate this paper to the memory of Dr. Robert Jack Cornett – a great professor, teacher and friend who is hugely missed by all those of us fortunate enough to have spent time under his inspirational tutelage and guidance.

Funding

The author(s) received no financial support for the research, authorship, and/or publication of this article.

ORCID iD

Simon Hayles https://orcid.org/0000-0001-8266-8263

References

Asikainen CA and Werle SF (2007) Accretion of ferromanganese nodules that form pavement in Second Connecticut Lake, New Hampshire. *Proceedings of the National Academy of Sciences* 104(45): 17579–17581.

Balzer SA and Broster BE (1994) Comparison of clast and matrix dispersal in till: Canterbury area, New Brunswick. *Atlantic Geology* 30(1): 9–17.

Beals HL (1966) Manganese-iron concretions in Nova Scotia lakes. *Atlantic Geology* 2(2): 70–72.

Belzile N, Chen YW and Grenier M (2001) Freshwater metallic concretions from an acidic lake characterized by X-ray energy dispersive spectrometry. *Canadian journal of analytical sciences and spectroscopy* 46(5): 145–151.

Belzile N and Tessier A (1990) Interactions between arsenic and iron oxyhydroxides in lacustrine sediments. *Geochimica et Cosmochimica Acta* 54(1): 103–109.

Boudreau BP (1988) Mass-transport constraints on the growth of discoidal ferromanganese nodules. *American Journal of Science* 288: 777–797.

Boudreau BP (1999) Metals and models: diagenic modelling in freshwater lacustrine sediments. *Journal of Paleolimnology* 22(3): 227–251.

Broster BE and Dickinson PJ (2015) Late Wisconsinan and Holocene development of Grand Lake Meadows area and southern reaches of the Saint John River Valley, New Brunswick, Canada. *Atlantic Geology* 51(1): 206–220.

Broster BE and Seaman AA (1991) Glacigenic rafting of weathered granite: Charlie Lake, New Brunswick. *Canadian Journal of Earth Sciences* 28(4): 649–654.

Brugam RB, McKeever K and Kolesa L (1998) A diatom-inferred water depth reconstruction for an Upper Peninsula, Michigan, lake. *Journal of Paleolimnology* 20(3): 267–276.

Callender E (1973) Geochemistry of Ferromanganese Crusts, Manganese Carbonate Crusts, and Associated Ferromanganese Nodules from Green Bay, Lake Michigan. NTIS Rep. No. PB-223 156-10/SL. National Science Foundation and US Dept. of Energy Rep. No. NSF/DOE-73-15-10.

Calvert SE and Price NB (1970) Composition of manganese nodules and manganese carbonates from Loch Fyne, Scotland. *Contributions to Mineralogy and Petrology* 29(3): 215–233.

Calvert SE and Price NB (1977) Shallow water, continental margin and lacustrine nodules: distribution and geochemistry. In: *Elsevier Oceanography series*, Vol.15. Amsterdam: Elsevier, pp.45–86.

Chapnick SD, Moore WS and Nealson KH (1982) Microbially mediated manganese oxidation in a freshwater lake1. *Limnology and Oceanography* 27(6): 1004–1014.

Couture RM, Gobeil C and Tessier A (2010) Arsenic, iron and sulfur co-diagenesis in lake sediments. *Geochimica et Cosmochimica Acta* 74(4): 1238–1255.

Crerar DA and Barnes HL (1974) Deposition of deep-sea manganese nodules. *Geochimica et Cosmochimica Acta* 38(2): 279–300.

Cronan DS and Thomas RL (1970) Ferromanganese concretions in Lake Ontario. *Canadian Journal of Earth Sciences* 7(5): 1346–1349.

Dangeti S, Roshani B, Rindall B et al. (2017) Biofiltration field study for cold Fe(II)- and Mn(II)-rich groundwater: accelerated Mn(II) removal kinetics and cold-adapted Mn(II)-oxidizing microbial populations. *Water Quality Research Journal* 52(4): 229–242.

Dauval'ter VA and Il'yashuk BP (2007) Conditions of formation of ferromanganese nodules in the bottom sediments of lakes in the Baltic shield. *Geochemistry International* 45(6): 615–619.

Davis M, Douglas C, Calcote R et al. (2000) Holocene climate in the western Great Lakes national parks and lakeshores: implications for future climate change. *Conservation Biology* 14(4): 968–983.

Davison W (1993) Iron and manganese in lakes. *Earth-Science Reviews* 34(2): 119–163.

Davison W and Seed G (1983) The kinetics of the oxidation of ferrous iron in synthetic and natural waters. *Geochimica et Cosmochimica Acta* 47(1): 67–79.

Dean WE (1970) Fe-Mn oxidate crusts in Oneida Lake, New York. In: *Proc. conf. great lakes res* (Vol.13, pp.217–226). New York, NY.

Dean WE, Ahlbrandt TS, Anderson RY et al. (1996) Regional aridity in North America during the middle Holocene. *The Holocene* 6(2): 145–155.

DiChristina TJ and DeLong EF (1993) Design and application of rRNA-targeted oligonucleotide probes for the dissimilatory iron- and manganese-reducing bacterium Shewanella putrefaciens. *Applied and Environmental Microbiology* 59(12): 4152–4160.

Dostal J, van Hengstum TR, Shellnutt JG et al. (2016) Petrogenetic evolution of Late Paleozoic rhyolites of the Harvey Group, southwestern New Brunswick (Canada) hosting uranium mineralization. *Contributions to Mineralogy and Petrology* 171(6): 59.

Downs RT and Hall-Wallace M (2003) The American Mineralogist Crystal Structure Database. *American Mineralogist* 88: 247–250.

Dranga SA, Hayles S and Gajewski K (2018) Synthesis of limnological data from lakes and ponds across Arctic and Boreal Canada. *Arctic Science* 4(2): 167–185.

Edgington DN and Callender E (1970) Minor element geochemistry of Lake Michigan ferromanganese nodules. *Earth and Planetary Science Letters* 8(2): 97–100.

Erbs M and Spain J (2002) Microbial iron metabolism in natural environments. *Microbial Diversity* 2002: 1–9.

Fortin D, Ferris FG and Beveridge TJ (1997) Surface-mediated mineral development by bacteria. *Reviews in mineralogy and geochemistry* 35(1): 161–180.

Froelich PN, Klinkhammer GP, Bender ML et al. (1979) Early oxidation of organic matter in pelagic sediments of the eastern equatorial Atlantic: suboxic diagenesis. *Geochimica et Cosmochimica Acta* 43(7): 1075–1090.

Fyffe LR, Lutes GG and St. Peter CJ (2005) Bedrock Geology of the McAdam area (NTS 21 G/11), York County, New Brunswick. New Brunswick Department of Natural Resources. Minerals, Policy and Planning Division. *Plate* 2005-34.

Gasparatos D (2013) Sequestration of heavy metals from soil with Fe–Mn concretions and nodules. *Environmental Chemistry Letters* 11(1): 1–9.

German CR and Elderfield H (1989) Rare earth elements in Saanich Inlet, British Columbia, a seasonally anoxic basin. *Geochimica et Cosmochimica Acta* 53(10): 2561–2571.

Ghiorse WC (1984) Biology of iron-and manganese-depositing bacteria. *Annual Review of Microbiology* 38(1): 515–550.

Gillette NJ (1961) Oneida Lake pancakes. New York State Conservationist 18: 41.

Glasby GP (1973) Mechanisms of enrichment of the rarer elements in marine manganese nodules. *Marine Chemistry* 1(2): 105–125.

Glasby GP, Emelyanov EM, Zhamoida VA et al. (1997) Environments of formation of ferromanganese concretions in the Baltic Sea: a critical review. *Geological Society London Special Publications* 119(1): 213–237.

Gorham E and Swaine DJ (1965) The influence of oxidizing and reducing conditions upon the distribution of some elements in lake sediments1. *Limnology and Oceanography* 10(2): 268–279.

Gounot AM (1994) Microbial oxidation and reduction of manganese: consequences in groundwater and applications. *FEMS Microbiology Reviews* 14: 339–349.

Government of New Brunswick (2020) Department of Environment and Local Government Lake Water Quality Data. Available at: https://www.elgegl.gnb.ca/LakesNB-NBLacs/en/SamplingLocation/Index (accessed 28 August 2020).

Gregory E and Staley JT (1982) Widespread distribution of ability to oxidize manganese among freshwater bacteria. *Applied and Environmental Microbiology* 44(2): 509–511.

Grigoriev AG, Zhamoida VA and Glasby GP (2004) Distribution of radionuclides in ferromanganese concretions and associated sediments from the northern-eastern Gulf of Finland. *Baltica* 17(2): 63–70.

Hawks RC and Troup AG (1970) Chemistry and origin of freshwater ferromanganese concretions. *Limnology and Oceanography* 15: 702–712.

Honig CA and Scott DB (1987) Postglacial stratigraphy and sea-level change in southwestern New Brunswick. *Canadian Journal of Earth Sciences* 24(2): 354–364.

Jackson ST and Booth RK (2002) The role of Late Holocene climate variability in the expansion of yellow birch in the western Great Lakes region. *Diversity and Distributions* 8(5): 275–284.

Jansen E, Andersson C, Moros M et al. (2008) The early to mid-Holocene thermal optimum in the North Atlantic. In: Battarbee BY, Binney RW, HA, (eds) *Natural Climate Variability and Global Warming–A Holocene Perspective*. Chichester: Wiley-Blackwell, pp.123–137.

Jansen E, Overpeck J, Briffa KR et al. (2007) Palaeoclimate. In: Climate Change 2007: The Physical Science Basis. Contribution of Working Group I to the Fourth Assessment Report of the Intergovernmental Panel on Climate Change. Cambridge: Cambridge University Press, pp.433–497.

Karmakar M, Leavitt PR and Cumming BF (2015) Enhanced algal abundance in northwest Ontario (Canada) lakes during the warmer early-to mid-Holocene period. *Quaternary Science Reviews* 123: 168–179.

Kaufman DS, Axford YL, Henderson ACG et al. (2016) Holocene climate changes in eastern Beringia (NW North America) – A systematic review of multi-proxy evidence. *Quaternary Science Reviews* 147: 312–339.

Kieser WE, Zhao X-L, Clark ID et al. (2015) The André E. Lalonde AMS Laboratory – The new accelerator mass spectrometry facility at the University of Ottawa. *Nuclear Instruments & Methods in Physics Research Section B, Beam Interactions with Materials and Atoms* 361: 110–114.

Kindle EM (1935) Manganese concretions in Nova Scotia lakes. *Transactions of the Royal Society of Canada* 29: 163–180.

Krishnaswami S and Moore WS (1973) Accretion rates of freshwater manganese deposits. *Nature Physical Science* 243(129): 114–116.

Laird KR and Cumming BF (2008) Reconstruction of Holocene Lake level from diatoms, chrysophytes and organic matter in a drainage lake from the Experimental Lakes Area (northwestern Ontario, Canada). *Quaternary Research* 69(2): 292–305.

Lavoie M and Richard PJH (2000) Postglacial water-level changes of a small lake in southern Québec, Canada. *The Holocene* 10(5): 621–634.

Lee S, Shen Z and Xu H (2016) Study on nanophase iron oxyhydroxides in freshwater ferromanganese nodules from Green Bay, Lake Michigan, with implications for the adsorption of As and heavy metals. *American Mineralogist* 101(9): 1986–1995.

Lee S and Xu H (2016) XRD and TEM studies on nanophase manganese oxides in freshwater ferromanganese nodules from Green Bay, Lake Michigan. *Clays and Clay Minerals* 64(5): 523–536.

Leonard PRR, Lentz DR and Poujol M (2006) Petrology, geochemistry, and U-Pb (zircon) age of the quartz-feldspar porphyry dyke at the Lake George antimony mine, New Brunswick: implications for origin, emplacement process, and mineralization. *Atlantic Geology* 42(1): 13–29.

Lewis CF, Forbes DL, Todd BJ et al. (2001) Uplift-driven expansion delayed by middle Holocene desiccation in Lake Winnipeg, Manitoba, Canada. *Geology* 29(8): 743–746.

Leybourne MI and Johannesson KH (2008) Rare earth elements (REE) and yttrium in stream waters, stream sediments, and Fe–Mn oxyhydroxides: fractionation, speciation, and controls over REE+Y patterns in the surface environment. *Geochimica et Cosmochimica Acta* 72(24): 5962–5983.

Little BJ, Wagner PA and Lewandowski Z (1997) Spatial relations between bacteria and metal surfaces. *Reviews in mineralogy* 35: 123–159.

Liu YG, Miah MR and Schmitt RA (1988) Cerium: a chemical tracer for paleo-oceanic redox conditions. *Geochimica et Cosmochimica Acta* 52(6): 1361–1371.

Lutes GG (1987) Geology and geochemistry of the Pokiok Batholith, New Brunswick (Vol. 22). Minerals and Energy Division, Dept. of Natural Resources and Energy, Government of Canada.

Lysyuk GN (2008) Biomineral nanostructures of manganese oxides in oceanic ferromanganese nodules. *Geology of Ore Deposits* 50(7): 647–649.

MacRae ND, Nesbitt HW and Kronberg BI (1992) Development of a positive Eu anomaly during diagenesis. *Earth and Planetary Science Letters* 109(3-4): 585–591.

Manheim FT (1965) Manganese-iron accumulations in the shallow marine environment. *Occasional Publication of Narragansett Marine Laboratory* 3: 217–276.

Marcott SA, Shakun JD, Clark PU et al. (2013) A reconstruction of regional and global temperature for the past 11,300 years. *Science* 339(6124): 1198–1201.

Martin ST (2005) Precipitation and dissolution of iron and manganese oxides. *Environmental Catalysis* 1: 61–82.

McLennan SM (1989) Rare earth elements in sedimentary rocks: influence of provenance and sedimentary processes. In: Lipin BR and McKay GA (eds) *Geochemistry and Mineralogy of Rare Earth Elements*. Washington, DC: Mineral. Soc. Am, pp.169–200.

Medcof JC (1979) Iron-manganese concretions from New Brunswick Lakes. *Journal of the New Brunswick Museum* 125–131.

Millero FJ, Sotolongo S and Izaguirre M (1987) The oxidation kinetics of Fe(II) in seawater. *Geochimica et Cosmochimica Acta* 51(4): 793–801.

Moore W, Dean W, Krishnaswami S et al. (1980) Growth rates of manganese nodules in Oneida Lake, New York. *Earth and Planetary Science Letters* 46(2): 191–200.

Moos MT, Laird KR and Cumming BF (2009) Climate-related eutrophication of a small boreal lake in northwestern Ontario: a palaeolimnological perspective. *The Holocene* 19(3): 359–367.

Moss B, Kosten S, Meerhoff M et al. (2011) Allied attack: climate change and eutrophication. *Inland Waters* 1(2): 101–105.

Mott RJ (1975) Palynological studies of lake sediment profiles from southwestern New Brunswick. *Canadian Journal of Earth Sciences* 12(2): 273–288.

Mullins HT (1998) Environmental change controls of lacustrine carbonate, Cayuga Lake, New York. *Geology* 26(5): 443–446.

Nayak B, Das SK and Munda P (2013) Biogenic signature and ultra microfossils in ferromanganese nodules of the Central Indian Ocean Basin. *Journal of Asian Earth Sciences* 73: 296–305.

Nealson KH and Myers CR (1992) Microbial reduction of manganese and iron: new approaches to carbon cycling. *Applied and Environmental Microbiology* 58(2): 439.

Odegaard C, Rea DK and Moore TC (2003) Stratigraphy of the mid-Holocene black bands in Lakes Michigan and Huron: Evidence for possible basin-wide anoxia. *Journal of Paleolimnology* 29(2): 221–234.

Patterson RT, Mazzella V, Macumber AL et al. (2020) A novel protocol for mapping the spatial distribution of storm derived sediment in lakes. *SN Applied Sciences* 2(12): 1–16.

Pierce ML and Moore CB (1982) Adsorption of arsenite and arsenate on amorphous iron hydroxide. *Water Research* 16(7): 1247–1253.

Piper DZ (1974) Rare earth elements in ferromanganese nodules and other marine phases. *Geochimica et Cosmochimica Acta* 38(7): 1007–1022.

Post JE (1999) Manganese oxide minerals: Crystal structures and economic and environmental significance. *Proceedings of the National Academy of Sciences* 96(7): 3447–3454.

Price NB and Calvert SE (1970) Compositional variation in Pacific Ocean ferromanganese nodules and its relationship to sediment accumulation rates. *Marine Geology* 9(3): 145–171.

Quinlan G and Beaumont C (1981) A comparison of observed and theoretical postglacial relative sea level in Atlantic Canada. *Canadian Journal of Earth Sciences* 18(7): 1146–1163.

Rai D, Sass BM and Moore DA (1987) Chromium(III) hydrolysis constants and solubility of chromium(III) hydroxide. *Inorganic Chemistry* 26(3): 345–349.

Raven KP, Jain A and Loeppert RH (1998) Arsenite and arsenate adsorption on ferrihydrite: Kinetics, equilibrium, and adsorption envelopes. *Environmental Science & Technology* 32(3): 344–349.

R Core Team (2015) *R: A Language and Environment for Statistical Computing*. Vienna, Austria: R Foundation for Statistical Computing, http://www.R-project.org/

Reimer PJ, Brown TA and Reimer RW (2004) Discussion: reporting and calibration of post-bomb 14C data. *Radiocarbon* 46(3): 1299–1304.

Root RA, Dixit S, Campbell KM et al. (2007) Arsenic sequestration by sorption processes in high-iron sediments. *Geochimica et Cosmochimica Acta* 71(23): 5782–5803.

Rossmann R and Callender E (1968) Manganese nodules in Lake Michigan. *Science* 162(3858): 1123–1124.

Ryan RJ, Boehner RC and Calder JH (1991) Lithostratigraphic revisions of the Upper Carboniferous to Lower Permian strata in the Cumberland Basin, Nova Scotia and the regional implications for the Maritimes Basin in Atlantic Canada. *Bulletin of Canadian Petroleum Geology* 39(4): 289–314.

Sass BM and Rai D (1987) Solubility of amorphous chromium(III)-iron(III) hydroxide solid solutions. *Inorganic Chemistry* 26(14): 2228–2232.

Schoettle M and Friedman GM (1971) Fresh water iron-manganese nodules in Lake George, New York. *Geological Society of America Bulletin* 82(1): 101–110.

Scott DB, Brown K, Collins ES et al. (1995) A new sea-level curve from Nova Scotia: evidence for a rapid acceleration of sea-level rise in the late mid-Holocene. *Canadian Journal of Earth Sciences* 32(12): 2071–2080.

Šegvić B, Girardclos S, Zanoni G et al. (2018) Origin and paleoenvironmental significance of Fe Mn nodules in the Holocene perialpine sediments of Geneva Basin, western Switzerland. *Applied Clay Science* 160: 22–39.

Shaw J, Gareau P and Courtney R (2002) Palaeogeography of Atlantic Canada 13–0kyr. *Quaternary Science Reviews* 21(16-17): 1861–1878.

Solomina ON, Bradley RS, Hodgson DA et al. (2015) Holocene glacier fluctuations. *Quaternary Science Reviews* 111: 9–34.

Sommers MG, Dollhopf ME and Douglas S (2002) Freshwater ferromanganese stromatolites from Lake Vermilion, Minnesota: microbial culturing and environmental scanning electron microscopy investigations. *Geomicrobiology Journal* 19(4): 407–427.

Sozanski AG and Cronan DS (1976) Environmental differentiation of morphology of ferromanganese oxide concretion in Shebandowan Lakes, Ontario1. *Limnology and Oceanography* 21(6): 894–898.

Sozanski AG and Cronan DS (1979) Ferromanganese concretions in Shebandowan Lakes, Ontario. *Canadian Journal of Earth Sciences* 16(1): 126–140.

St-Jean G, Kieser WE, Crann CA et al. (2017) Semi-Automated Equipment for CO2 purification and graphitization at the A.E. Lalonde AMS Laboratory (Ottawa, Canada). *Radiocarbon* 59(3): 941–956.

St. Clair B, Pottenger J, Debes R et al. (2019) Distinguishing biotic and abiotic iron oxidation at low temperatures. *ACS Earth and Space Chemistry* 3(6): 905–921.

St. Peter C (1993) Maritimes Basin evolution: key geologic and seismic evidence from the Moncton Subbasin of New Brunswick. *Atlantic Geology* 29(3): 233–270.

Stein LY, La Duc MT, Grundl TJ et al. (2001) Bacterial and archaeal populations associated with freshwater ferromanganous micronodules and sediments. *Environmental Microbiology* 3(1): 10–18.

Stuiver M and Polach HA (1977) Discussion reporting of 14C Data. *Radiocarbon* 19(3): 355–363.

Suess E and Djafari D (1977) Trace metal distribution in Baltic Sea ferromanganese concretions: inferences on accretion rates. *Earth and Planetary Science Letters* 35(1): 49–54.

Takamatsu T, Kawai T and Nishikawa M (2000) Elemental composition of short sediment cores and ferromanganese concretions from Lake Baikal. In: *Lake Baikal*. Amsterdam: Elsevier, pp.155–164.

Takamatsu T, Kawashima M, Matsushita R et al. (1985) General distribution profiles of thirty-six elements in sediments and manganese concretions of Lake Biwa. *Japanese Journal of Limnology (Rikusuigaku Zasshi)* 46(2): 115–127.

Tebo BM, Bargar JR, Clement BG et al. (2004) Biogenic manganese oxides: properties and mechanisms of formation. *Annual Review of Earth and Planetary Sciences* 32: 287–328.

Tebo BM, Johnson HA, McCarthy JK et al. (2005) Geomicrobiology of manganese(II) oxidation. *Trends in Microbiology* 13(9): 421–428.

Tessier A, Fortin D, Belzile N et al. (1996) Metal sorption to diagenetic iron and manganese oxyhydroxides and associated organic matter: narrowing the gap between field and laboratory measurements. *Geochimica et Cosmochimica Acta* 60(3): 387–404.

Tessier A, Rapin F and Carignan R (1985) Trace metals in oxic lake sediments: possible adsorption onto iron oxyhydroxides. *Geochimica et Cosmochimica Acta* 49(1): 183–194.

Trivedi P, Dyer JA and Sparks DL (2003) Lead sorption onto ferrihydrite. 1. A macroscopic and spectroscopic assessment. *Environmental Science & Technology* 37(5): 908–914.

Trudinger PA and Swaine DJ (1979) *Biogeochemical Cycling of Mineral-Forming Elements*. Amsterdam: Elsevier.

Tufano KJ, Reyes C, Saltikov CW et al. (2008) Reductive processes controlling arsenic retention: revealing the relative importance of iron and arsenic reduction. *Environmental Science & Technology* 42(22): 8283–8289.

Tully BJ and Heidelberg JF (2013) Microbial communities associated with ferromanganese nodules and the surrounding sediments. *Frontiers in Microbiology* 4: 161.

Tyler P and Buckney R (1980) Ferromanganese concretions in Tasmanian lakes. *Marine and Freshwater Research* 31(4): 525–531.

Utting J, Giles PS and Dolby G (2010) Palynostratigraphy of Mississippian and Pennsylvanian rocks, Joggins area, Nova Scotia and New Brunswick, Canada. *Palynology* 34(1): 43–89.

Vitre RD, Belzile N and Tessier A (1991) Speciation and adsorption of arsenic on diagenetic iron oxyhydroxides. *Limnology and Oceanography* 36(7): 1480–1485.

Walker M, Gibbard P, Head MJ et al. (2019) Formal subdivision of the Holocene series/epoch: a summary. *Journal of the Geological Society of India* 93(2): 135–141.

Wang XH, Schloßmacher U, Natalio F et al. (2009) Evidence for biogenic processes during formation of ferromanganese crusts from the Pacific Ocean: implications of biologically induced mineralization. *Micron* 40(5-6): 526–535.

Wehrli B, Sulzberger B and Stumm W (1989) Redox processes catalyzed by hydrous oxide surfaces. *Chemical Geology* 78(3-4): 167–179.

Wei T, Simko V, Levy M et al. (2017) Package 'corrplot'. *Statistician* 56(316): e24.

Whalen JB, Fyffe LR, Longstaffe FJ et al. (1996) The position and nature of the Gander–Avalon boundary, southern New Brunswick, based on geochemical and isotopic data from granitoid rocks. *Canadian Journal of Earth Sciences* 33(2): 129–139.

Whalen JB, Jenner GA, Currie KL et al. (1994) Geochemical and isotopic characteristics of granitoids of the Avalon Zone, southern New Brunswick: possible evidence for repeated delamination events. *The Journal of Geology* 102(3): 269–282.

Williams TM and Owen RB (1992) Geochemistry and origins of lacustrine ferromanganese nodules from the Malawi Rift, Central Africa. *Geochimica et Cosmochimica Acta* 56(7): 2703–2712.

Yang XM, Lentz DR, Chi G et al. (2008) Geochemical characteristics of gold-related granitoids in southwestern New Brunswick, Canada. *Lithos* 104(1-4): 355–377.

Young LB and Harvey HH (1992) The relative importance of manganese and iron oxides and organic matter in the sorption of trace metals by surficial lake sediments. *Geochimica et Cosmochimica Acta* 56(3): 1175–1186.

Yu Z, McAndrews JH and Eicher U (1997) Middle Holocene dry climate caused by change in atmospheric circulation patterns: evidence from lake levels and stable isotopes. *Geology* 25(3): 251–254.

Yu Z and McAndrews JH (1994) Holocene water levels at Rice Lake, Ontario, Canada: sediment, pollen and plant-macrofossil evidence. *The Holocene* 4(2): 141–152.